ICLASS 2009, 11th Triennial International Annual Conference on Liquid Atomization and Spray Systems, Vail, Colorado USA, July 2009

Detailed numerical investigation of turbulent atomization of liquid jets

Olivier Desjardins*
Department of Mechanical Engineering
University of Colorado, Boulder, CO 80309-0427

Abstract

A detailed numerical investigation of turbulent liquid jets in quiescent air is conducted, with focus on the processes leading to liquid atomization. Spectral refinement of the interface is employed to provide an accurate description of the phase-interface, even at the sub-cell level. The ghost fluid method is used to handle the different material properties of the phases and the surface tension force in a sharp manner. A temporally evolving turbulent planar jet is simulated for several values of the Reynolds and Weber numbers, and statistics are extracted. Direct visualization of the flow structures allows to lay out a clear picture of the atomization process. Early interface deformation is caused by turbulent eddies that carry enough kinetic energy to overcome surface tension forces. Then, liquid protrusions are stretched out into ligaments that rupture following Rayleigh's theory or due to aerodynamic forces. This numerical study provides a wealth of much-needed detailed information on the turbulent atomization process, which is invaluable to large eddy simulation modeling.

Introduction

The objective of this work is to improve the understanding of primary atomization of turbulent liquid jets through detailed numerical simulations. For this problem to become numerically tractable, several key ingredients are combined. Since the Reynolds number associated with atomization is generally high, numerical schemes have to be tailored for the simulation of turbulence. For this purpose, an arbitrarily high order conservative finite difference scheme for variable density, low Mach number flows is used [1]. Combining this scheme with the Ghost Fluid Method (GFM), the discontinuous material properties encountered in multiphase flows can be robustly handled. Also, the surface tension force, which is singular in nature, is considered in a more accurate way. In order to correctly represent the phase-interface geometry, spectral refinement of a level set function is introduced [2]. Thanks to a sub-cell polynomial reconstruction of the level set function, this approach provides great accuracy even for poorly resolved interface structures, while the use of a narrow-band formulation and semi-Lagrangian transport leads to a limited cost. This method is found appropriate for simulating primary atomization because of the excellent resolution it provides.

This numerical approach is applied in a detailed study of the turbulent atomization process characteristic of Diesel injection. The density ratio employed is similar to that of Diesel injection. The Reynolds number is slightly reduced compared to realistic injectors, but still of the right order of magnitude. The Weber number is strongly reduced in order to make the liquid structures tractable. A temporally evolving turbulent planar jet is simulated for several values of the Reynolds and Weber numbers, and statistics are extracted. Direct visualization of the flow structures allows to lay out a clear picture of the atomization process. Early interface deformation is caused by turbulent eddies that carry enough kinetic energy to overcome surface tension forces. Then, liquid protrusions are stretched out into ligaments that rupture following Rayleigh's theory or due to aerodynamic forces. Due to the limited length of this paper, only mean streamwise velocity statistics are reported.

Flow configuration

The flow considered in this section consists of a temporally evolving planar liquid jet in quiescent air. Figure 1(a) shows a sketch of the flow configuration. The liquid jet is initially of height H, and its bulk velocity is U_0. The computational domain is periodic in the streamwise and spanwise directions, x and z respectively, while in the y direction, a symmetry condition is employed. The $4H \times 6H \times 4H$ domain is discretized on a $256 \times 384 \times 256$ uniform mesh, leading to $\Delta x = \Delta y = \Delta z = H/64$. The initial velocity is

* *E-mail address:* desjardi@colorado.edu

obtained from a precursor simulation of a periodic channel flow. This precursor simulation is conducted in a $4H \times H \times 4H$ domain, discretized on a $256 \times 192 \times 256$ mesh, using the liquid material properties. Once the flow is established, *i.e.* once the friction coefficient reaches a constant value, the simulation is stopped and the velocity field is recorded. This field is then interpolated on the jet mesh to initialize the velocity in the region $-H/2 < y < H/2$, while the velocity outside of this region is set to zero. Even though the initial co-existence between a turbulent liquid and a still gas is a greatly simplified representation of turbulent liquid injection, the presence of realistic turbulence ensures that the planar jet destabilizes and develops rapidly. Throughout this work, time $t^\star$ will be non-dimensionalized using $t = t^\star U_0/H$.

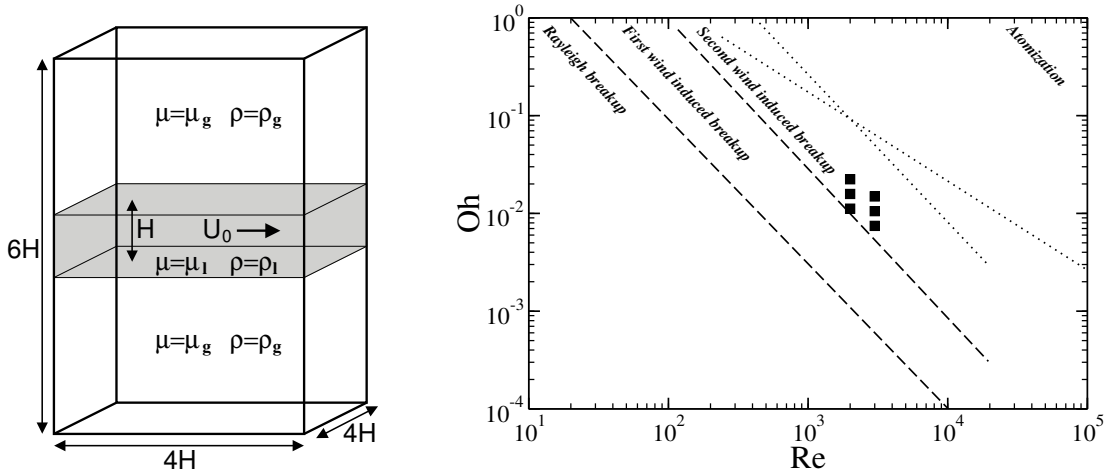

(a) Schematics of the temporally evolving planar jet.

(b) Cases considered in this work (symbols, see Table 1 for details) placed on the Ohnesorge chart for liquid jet breakup.

Figure 1. Flow configuration and parameters.

Case	ρ_l/ρ_g	μ_l/μ_g	Re	We	Oh
$TPa1$	40	40	3000	500	0.007454
$TPa2$	40	40	2000	500	0.011180
$TPb1$	40	40	3000	1000	0.010541
$TPb2$	40	40	2000	1000	0.015811
$TPc1$	40	40	3000	2000	0.014907
$TPc2$	40	40	2000	2000	0.022361

Table 1. Flow parameters for the various planar jet simulations.

The parameters used for the simulations are summarized in Table 1. The density ratio is set to $\rho_l/\rho_g = 40$, which corresponds to what is typically observed in Diesel engines, and which is sufficiently low to avoid any numerical difficulties. The choice is made to take $\mu_l/\mu_g = 40$, leading to $\nu_l = \nu_g$. Both the Reynolds number, $\mathrm{Re} = \rho_l U_0 H/\mu_l$, and the Weber number, $\mathrm{We} = \rho_l U_0^2 H/\sigma$, are varied such that both the effect of turbulence and the effect of surface tension forces can be studied. The Ohnesorge number, $\mathrm{Oh} = \mu_l/\left(\rho_l H \sigma\right)^{1/2}$, is also reported in Table 1 for the various cases. Clearly, the Ohnesorge number remains small for all cases, meaning that the liquid viscosity should not play any significant role throughout the atomization process, which is expected to be the case for Diesel injection. Figure 1(b) places the different cases studied on the Ohnesorge chart, first introduced by Ohnesorge [3], then improved by Reitz [4], Lefebvre [5], and Miesse [6]. Note that all the cases considered here lie within the so-called second wind induced breakup regime. However, as noted by [5], a fully turbulent liquid jet will be immediately disrupted because of the non-zero vertical velocity component, leading to a global turbulent disintegration of the liquid. As a result, it is expected that the cases studied here will all undergo turbulent atomization.

Resolution considerations

In these simulations, resolution is assessed by directly evaluating the liquid mass conservation errors as a function of time, as shown in Fig. 2(a). Small mass loss should suggest that indeed most liquid structures are

properly resolved at all times. For all three Re = 3000 cases, which are expected to be the most challenging simulations in terms of resolution, the mass conservation errors are found to remain below 2% for $t < 30$. This value is considered here to be sufficiently small to confirm that the chosen numerical parameters lead to a properly resolved flow. In addition, the temporal evolution of the normalized streamwise momentum is shown in Fig. 2(b). Note that momentum conservation errors are larger than mass conservation errors, which can be explained by the fact that the liquid structures that become under-resolved and disappear from the flow solver mesh often carry a lot of momentum. However, the momentum conservation errors remain limited, of the order of 5% for We = 500, 10% for We = 1000, and 15% for We = 2000.

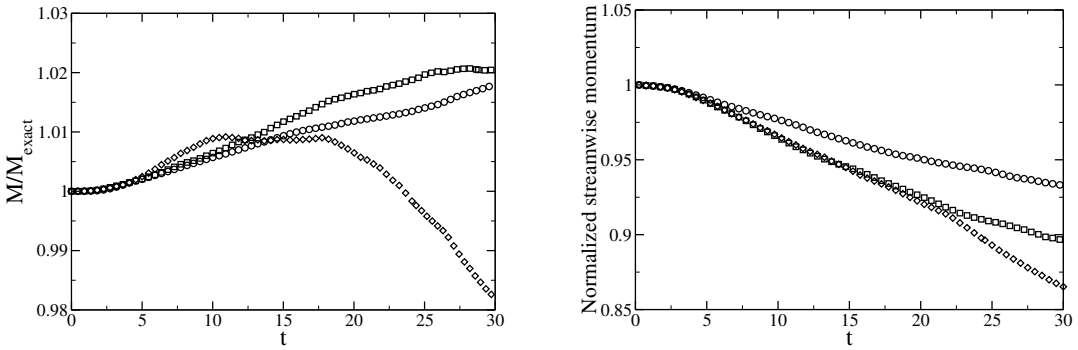

(a) Mass conservation errors (b) Momentum conservation errors

Figure 2. Temporal evolution of the normalized liquid mass (left) and normalized streamwise momentum (right) in the domain for Re = 3000: We = 500 (circles), We = 1000 (squares), and We = 2000 (diamonds).

Instantaneous results

Global description of the flow. In this section, the global features of the flow for jet $TPb1$ are first described. Figure 3 presents a three-dimensional view of the phase-interface at different times during the development of the liquid jet. As expected, because of the initially turbulent liquid, the interface starts wrinkling immediately after the beginning of the run. These corrugations then grow and complex phenomena become apparent, such as the entrapment of air bubbles within the liquid jet, or the wrapping of liquid sheets around eddies. As the interfacial structures become larger, individual ligaments are being stretched. Typically, they are found to be oriented in the $(-x)$-direction. These ligaments eventually rupture and form droplets. It should be noted that the disruption of the jet as well as the formation of droplets is dominated by these ligaments. The disruption of the jet does not display a cascade nature, where the jet would first breakup in big structures, then in smaller structures. The fact that most droplets are generated through the rupture of pre-existing ligaments is essential to the atomization process, and has been recurrently observed and documented [7]. From the results of these simulations, a clear picture of the atomization already emerges that can be summarized in three essential steps: (1) initial corrugation of the interface, (2) formation and stretching of liquid ligaments, and (3) rupture of these ligaments, leading to droplet formation.

It is interesting to note that Kelvin-Helmholtz (KH) instabilities are not observed at early times, and therefore, should not contribute to the first part of the jet development at $t < 10$. Yet, numerous droplets have already been generated. This suggests that the liquid turbulence plays an important role in the generation of the first droplets. As the jet keeps developing, a large scale KH type wave becomes visible, and greatly enhances the generation of ligaments, sheets, and droplets. However, this wave appears late in the simulation, and it might be caused by the confinement of the liquid jet, both in the streamwise and the lateral directions. The numerous liquid ligaments, crests, and droplets observed in the simulation results are qualitatively in good agreement with experimental observations by Faeth *et al.* [8].

Comparing the simulation results with experimental observations that have been reported in the literature, two main differences can be noted. First, Sallam *et al.* [9] reported that the ligaments they observed in their jets were randomly oriented, rather than preferentially oriented in the $(-x)$-direction. They attributed this fact to the small importance of aerodynamic forces in relationship with the large density ratio they were using. Here, because the density ratio is much lower, aerodynamic forces on the liquid structures are expected to be significant. The aerodynamic forces acting on the protruding liquid ligaments cause them to

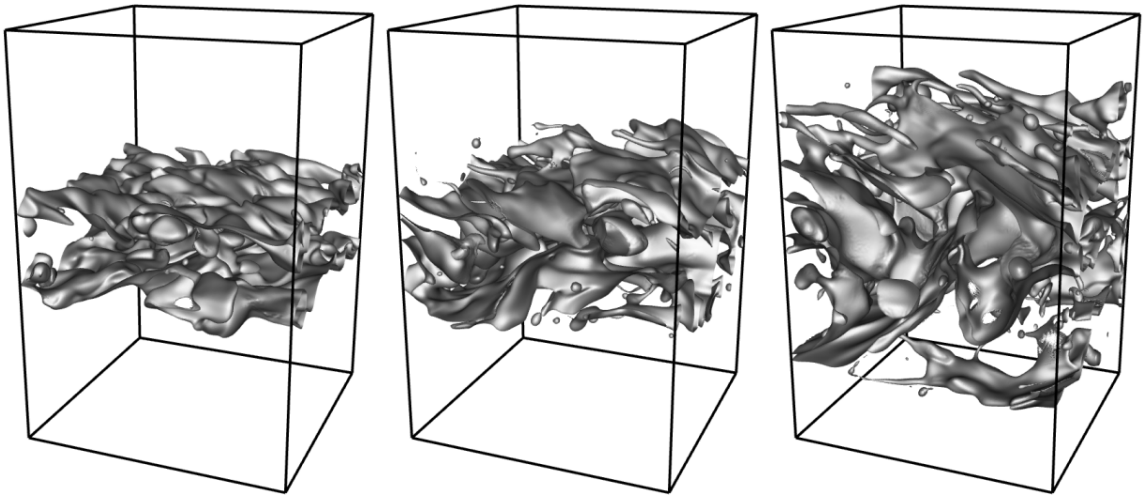

(a) $t = 7.5$ (b) $t = 17.5$ (c) $t = 27.5$

Figure 3. Instantaneous phase-interface location at different times for case $TPb1$.

be deflected towards the $(-x)$-direction, which was experimentally observed for a density ratio of the order of 100 by Wu and Faeth [10]. These differences are of great interest, since liquid atomization in many combustion devices, such as Diesel engines and gas turbines, involves such small density ratios. The present results might therefore be more relevant for these applications. Second, Sallam *et al.* [9] reported not observing any bubble in the region where the interface was sufficiently undisturbed to allow for direct visualization. In contrast the present simulations show gas bubbles trapped in the liquid. This difference could be caused again by aerodynamic effects in the simulations, or could be due to the nature of the turbulence in the liquid.

Effect of the Weber number. The effect of the surface tension forces is discussed by comparing a top view $(+y)$ of the interface at different Weber numbers. Cases $TPa1$, $TPb1$, and $TPc1$ are considered for this purpose. Figure 4 shows this top view at the times $t = 5$, 15, and 25. For the earliest time, a significant difference between the three interfacial shapes can be noted for the different Weber numbers. The interface roughness is much lower for We = 500 than for We = 2000, which is expected since surface tension forces work against the deformation of the interface. Clearly, at this time, the large scale structures are still very similar for the three different cases, indicating that the large scale turbulent eddies carry enough energy to induce interfacial deformation despite surface tension forces. Smaller scales become much more apparent for high Weber numbers, which suggests that surface tension forces act as a cut-off in interfacial structure length-scales. For high Weber number, even small turbulent scales, which carry less kinetic energy, can deform the interface, while for low Weber number, only energetic scales are able to disrupt the interface. The observation of the interfaces at later times confirms this analysis, and in general the low Weber number interface remains much less disturbed than the high Weber number interface. Note that similarities between the structures for various Weber numbers have mostly disappeared at $t = 15$. Regardless of the Weber number considered, droplets are generated through the creation and stretching of liquid ligaments. Ligaments are longer, thinner, and more numerous as the Weber number is increased. The same remark can be made concerning droplets, which tend to be smaller and more abundant for the high Weber number case than for the low Weber number. Finally, it should be noted that the sizes of ligaments and droplets become larger at later times in all cases, which has been observed also by Sallam *et al.* [9], and can be attributed to the dissipation of the small turbulent scales.

Effect of the Reynolds number. In order to assess the effect of the Reynolds number on the interface disruption, two different Reynolds numbers have been considered. While it is unclear whether many lasting differences will emerge between Re = 2000 and Re = 3000, the difference in the level of turbulence should at least impact the early deformation of the interface. Figure 5 compares the interface for cases $TPb1$ and $TPb2$ at different times throughout the simulations. Clearly, the later development of the various liquid structures is very similar between the two Reynolds numbers. The resulting ligaments appear to be of the same size, and the droplets seem similar in size and number. This observation suggests that the processes

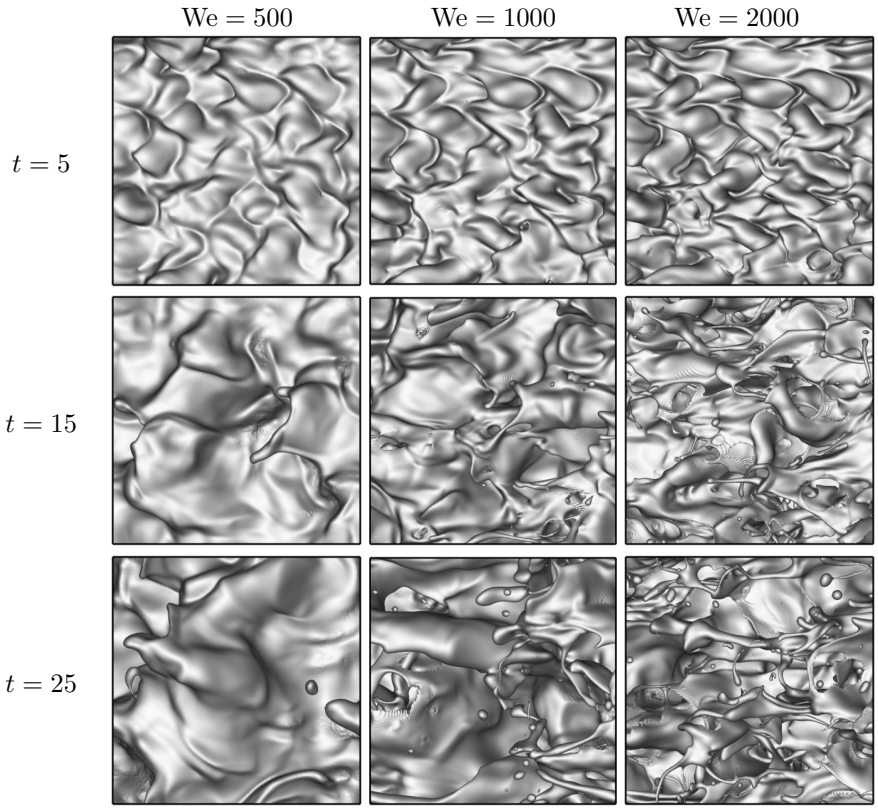

Figure 4. Top view of the interface for Re = 3000 as a function of time and Weber number.

by which ligaments are stretched out and ruptured are not significantly affected by changing the Reynolds number. Of course, the range of scales found in Re = 2000 turbulence and Re = 3000 turbulence is rather limited, therefore it is possible that changing the Reynolds number more significantly could have a stronger effect. Note that Sallam *et al.* [9] reported that increasing the injection velocity, *i.e.* increasing both the Reynolds number and the Weber number at the same time, led to little consequences on the largest liquid structures, while smaller and more numerous small scales were obtained. The main difference between the two simulations can be found in the earliest interface visualization, where the corrugation length scales appear larger for the low Reynolds number case. This is to be expected, considering that less energy is contained in small eddies for the low Reynolds number case compared to the larger Reynolds number case. Consequently, the early deformation on the smaller scales of the interface is more likely to take place on relatively larger length scales as the Reynolds number is reduced.

Statistical results

The mean longitudinal velocity is plotted at four different times for Re = 3000 and for various Weber numbers in Fig. 6. The velocity is normalized by the centerline velocity, and the y-coordinate is normalized by the jet half-width. With this normalization, a similar single-phase jet would show self-similar behavior in the time interval where a linear growth rate is observed. Here, it can be noted that the collapse of normalized profiles at different times is not perfect, especially for the low Weber number case, for which surface tension effects are stronger. However, for high Weber numbers, it appears that the velocity profiles collapse rather well, which suggests that two-phase jets display a self-similar nature when surface tension forces are not dominating.

Conclusion

This work attempts to improve the understanding of primary atomization through detailed numerical simulations. Numerical techniques have matured rapidly in the past few years, and the associated increase in

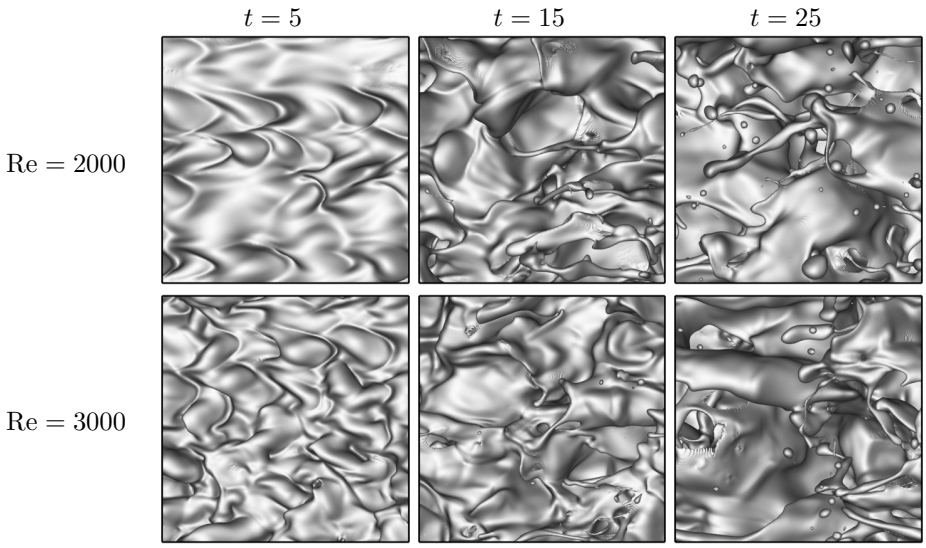

Figure 5. Top view of the interface for We = 1000 as a function of time and Reynolds number.

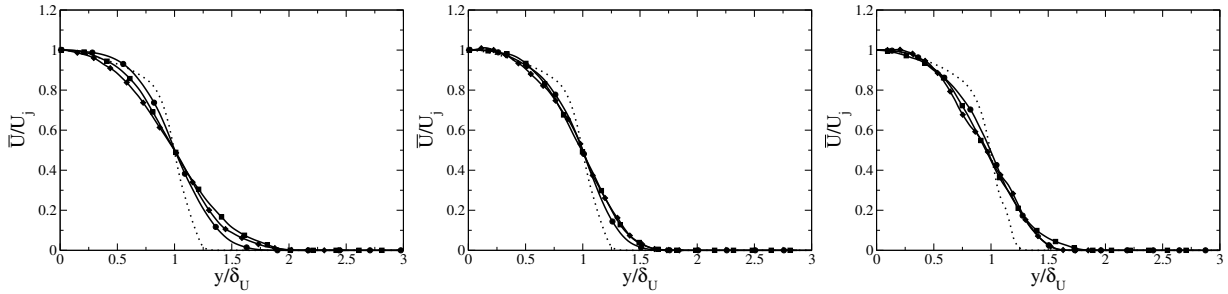

(a) We = 500 (b) We = 1000 (c) We = 2000

Figure 6. Mean profiles of streamwise velocity of the planar jets at different times for Re = 3000 and various Weber numbers: $t = 1$ (dotted line), $t = 10$ (circles), $t = 20$ (squares), and $t = 30$ (diamonds).

computational power allows to perform fine simulations of complex turbulent problems. By carefully choosing the simulation parameters, turbulent atomization can be simulated, with reasonable confidence in the numerics. This work is considered a first step towards realistic applications. The density ratio employed is similar to that of Diesel injection. The Reynolds number is slightly reduced compared to realistic injectors, however still of the right order of magnitude. The Weber number is reduced manyfold, in order to make the liquid structures tractable. This numerical study provides a wealth of much-needed detailed information on the turbulent atomization process, which is invaluable to large eddy simulation modeling.

References

1. Desjardins, O., Blanquart, G., Balarac, G., and Pitsch, H., *J. Comput. Phys.* 227(15):7125–7159 (2008).
2. Desjardins, O. and Pitsch, H., *J. Comp. Phys.* 228(5):1658–1677 (2009).
3. Ohnesorge, W. *Z. Angew. Math. Mech.* 16:355–358 (1936).
4. Reitz, R. D. *Atomization and other breakup regimes of a liquid jet* PhD thesis Princeton University (1978).
5. Lefebvre, A. H. *Atomization and spray*, Taylor and Francis, 1989.
6. Miesse, C. C. *Ind. Eng. Chem.* 47:1690–1701 (1955).
7. Villermaux, E. *Ann. Rev. Fluid. Mech.* 39:419–446 (2007).
8. Faeth, G. M., Hsiang, L. P., and Wu, P. K., *International Journal of Multiphase Flow* 21:99–127 (1995).
9. Sallam, K. A., Dai, Z., and Faeth, G. M., *International Journal of Multiphase Flow* 25(6):1161–1180 (1999).
10. Wu, P. K. and Faeth, G. M., *Atomization and Sprays* 3(3):265–289 (1993).